Remote Sensing of Environment 184 (2016) 374–386

Contents lists available at ScienceDirect

Remote Sensing of Environment

journal homepage: www.elsevier.com/locate/rse

Land cover change detection by integrating object-based data blending model of Landsat and MODIS

Miao Lu [a], Jun Chen [b,*], Huajun Tang [a], Yuhan Rao [c], Peng Yang [a], Wenbin Wu [a,*]

[a] Key Laboratory of Agri-informatics, Ministry of Agriculture/Institute of Agricultural Resources and Regional Planning, Chinese Academy of Agricultural Sciences, Beijing 100081, China
[b] National Geomatics Centre of China, Beijing 100830, China
[c] Department of Geographical Sciences, University of Maryland, College Park, MD 20742, USA

ARTICLE INFO

Article history:
Received 9 October 2015
Received in revised form 1 July 2016
Accepted 19 July 2016
Available online 29 July 2016

Keywords:
Change detection
Object-based
Data blending
NDVI gradient difference
NDVI time series

ABSTRACT

Accurate information on land cover changes is critical for global change studies, land cover mapping and ecosystem management. Although there are numerous change detection methods, pseudo changes can occur if data are acquired from different seasons, which presents a significant challenge for land cover change detection. In this study, land cover change detection by integrating object-based data blending model of Landsat and MODIS is proposed to solve this issue. The Estimation of Scale Parameter (ESP) tool under Minimum Mapping Unit (MMU) restriction is employed to identify the optimal scale for Landsat image segmentation. The Object Based Spatial and Temporal Vegetation Index Unmixing Model (OB-STVIUM) disaggregates MODIS NDVIs to Landsat objects using the spatial analysis and the linear mixing theory. Then, the change detection method of NDVI Gradient Difference (NDVI-GD) is developed to detect change and no-change objects considering the NDVI shape and value differences simultaneously. The results of the study indicate that the approach proposed in this study can effectively detect change areas when Landsat images are acquired from different seasons. OB-STVIUM is more suitable for change detection application compared with the Spatial and Temporal Adaptive Reflectance Fusion Model (STARFM) and NDVI Linear Mixing Growth Model (NDVI-LMGM), because it is less sensitive to the number and acquisition time of Landsat images.

1. Introduction

Land cover composition and its changes play an important role in many scientific studies and socioeconomic assessments because they are essential inputs for global climate models (Bontemps et al., 2012a; Yang et al., 2013; Wu et al., 2014), primary references for ecosystem management (Mora et al., 2014; Sun et al., 2015), and fundamental information for understating coupled human and natural systems (Yu et al., 2013; Ban et al., 2015; Lu et al., 2016). Accurate and up-to-date information regarding land cover and its dynamics are increasingly necessary at different spatial and temporal scales (Chen et al., 2015a; Jin et al., 2013).

Remote sensing has become an important tool for gathering and monitoring land cover dynamics, and numerous algorithms have been developed for detecting land cover changes (Hansen and Loveland, 2012; Tewkesbury et al., 2015). One of the main issues in land cover change detection is how to accurately extract change areas while eliminating the pseudo changes caused by phenological differences and other extraneous factors (Chen et al., 2013; Jin et al., 2013; Chen et al., 2015b). Extraneous factors (e.g., atmospheric conditions, soil moisture, and water turbidity) can be avoided by using some appropriate algorithms with images acquired from the same sensor in the same season (Chen et al., 2013; Jin et al., 2013). However, when images are acquired from different seasons, pseudo changes caused by phenological differences are inevitable which presents a significant challenge for land cover change detection. Since NDVI Time series can accurately track the seasonal characteristics and capture information of vegetation phenology, using NDVI time series provides a potential solution to avoid the pseudo changes caused by phenological differences (Jia et al., 2014; Chen et al., 2015b). Most studies have used NDVI time series acquired by moderate resolution sensors (e.g., MODIS, SPOT-VGT, and AVHRR) for land cover change detection because of their frequent revisiting time (e.g., daily revisit) (Lhermitte et al., 2008). However, it is a challenge to detect changes at small scales or heterogeneous landscapes using moderate resolution data. Images from fine resolution sensors like Landsat could provide much more detailed spatial information (Boschetti et al., 2015; Hilker et al., 2009). Although the Landsat archive is open and free, it is difficult to obtain dense Landsat time series due to cloud contamination or revisit cycle limitation (Bontemps et al., 2008; Bontemps et al., 2012b). For example, Kovalskyy and Roy (2013) indicated that the probability of there being at least one cloud-free image in each of the three seasons in the year 2000 was 0.194, 0.742 and

* Corresponding authors.
E-mail addresses: lumiao0616@163.com (M. Lu), chenjun@nsdi.gov.cn (J. Chen), wuwenbin@caas.cn (W. Wu).

http://dx.doi.org/10.1016/j.rse.2016.07.028
0034-4257/

0.790 for Landsat 5 TM, Landsat 7 ETM + and both Landsat sensors combined respectively, and the probability for the year of 2010 was 0.332, 0.621 and 0.727. Therefore, the probability of there being at least one cloud-free image in each of the three seasons in both 2000 and 2010 is 0.262 (0.790×0.332), considering Landsat 7 ETM + scan line corrector failed. Therefore, the pseudo change caused by phenological differences is inevitable when using Landsat image for change detection.

In order to combine temporal advantages of MODIS time series and spatial advantages of Landsat image, several data blending methods combining Landsat and MODIS have been developed to generate high spatio-temporal resolution data, e.g., Spatial and Temporal Adaptive Reflectance Fusion Model (STARFM) (Gao et al., 2006), Weighted Linear System (WLS) of sub-pixel NDVI (Busetto et al., 2008), Enhanced STARFM (ESTARFM) (Zhu et al., 2010), Spatial and Temporal Reflectance Unmixing Model (STRUM) (Gevaert and García-Haro, 2015) and NDVI Linear Mixing Growth Model (NDVI-LMGM) (Rao et al., 2015). The blended high spatio-temporal resolution data could be used to monitor changes in land cover and eliminate pseudo changes caused by phenological differences. For example, Hilker et al. (2009) introduced a data blending model called the Spatial Temporal Adaptive Algorithm for mapping Reflectance Change (STAARCH) to detect forest disturbances based on Landsat and MODIS reflectance data. Chen et al. (2015b) used the NDVI-LMGM to identify land cover changes to update land cover data. However, these methods are generally pixel-based blending models, which are sensitive to registration errors (Coppin et al., 2004), and might have a blocky appearance resulted from different scales of the fused images (Pohl and Van Genderen, 1998; Zhang, 2010). These methods also typically ignore useful context information, thus leading to "salt and pepper" effects on the blended result (Gong et al., 2008; Im et al., 2008). On the contrary, Object Based Image Analysis (OBIA) is currently gaining more attentions. Compared with a pixel, an object is a group of homogeneous pixels that represent a meaningful object in the real world (Blaschke, 2010; Bodart et al., 2011; Hu et al., 2013; Boschetti et al., 2015), and contains richer information regarding the shape, context and spatial relationship of the object (Benz et al., 2004; Chen et al., 2012; Powers et al., 2012). The OBIA is less sensitive to registration errors and can effectively solve the "salt and pepper" effect (Chen et al., 2014; Hussain et al., 2013). Unfortunately, few studies have been performed to develop an object-based data blending method for detecting land cover changes (Ban and Jacob, 2013).

In this paper, an Object Based Spatial and Temporal Vegetation Index Unmixing Model (OB-STVIUM) is proposed to solve the issue of phenological differences for land cover change detection. OB-STVIUM disaggregates MODIS NDVI time series into Landsat objects using spatial analysis and linear mixing theory. Based on the NDVI time series of the objects, the NDVI Gradient Difference (NDVI-GD) is designed to calculate the change magnitude considering the shape and value differences of the NDVI time series. The performance of this approach has been tested using data of Liquan County, Shanxi Province, China. The results of OB-STVIUM have been compared with original MODIS NDVIs and Landsat NDVIs, while the accuracy of NDVI-GD has been evaluated using change/no-change error matrix.

2. Methodology

The proposed method of object-based data blending and change detection includes three steps (Fig. 1). The first step is the multi-data segmentation of Landsat images using the optimal scale parameter determined by Estimation of Scale Parameter (ESP) tool under Minimum Mapping Unit (MMU) restriction. The second step is employing OB-STVIUM to disaggregate MODIS NDVI time series to Landsat objects times series through a spatial analysis and the linear mixing theory. The last step is using NDVI-GD to calculate the change magnitude and determining change and no-change objects by threshold defined. Each step will be described in the following subsections.

2.1. Multi-data segmentation

Image segmentation is the foundation of the object-based data blending model. The eCognition software has been widely used for OBIA. In the software, the bottom up region-merging technique is used to divide the image into homogeneous objects consisting of spectrally similar and spatially adjacent pixels (Desclée et al., 2006). The fundamental idea of the segmentation is that starting with each pixel as the original image object, adjacent image objects are merged into a larger object until the heterogeneity exceeds the threshold defined by the scale parameter (Benz et al., 2004; Desclée et al., 2006).

The most critical step of segmentation is determining the optimal segmentation scale. The ESP tool under MMU restriction is applied to select the optimal scale for segmentation (Fig. 1(a)). After a range of possible scale parameters are selected by the ESP tool, the size of objects for each scales are calculated, and then the optimal scale parameter is determined using the criterion of 'quantile-5' object with the pre-defined MMU. ESP is an automatic tool programmed in Cognition Network Language to determine the most suitable series of scale parameters in the eCognition software (Drăguţ et al., 2010). The fundamental idea of ESP is to select the segmentation scales based on the Rate of Change (ROC) curve for the calculated Local Variance (LV) of object heterogeneity at various scales (see left panel in Fig. 1(a)). The scales corresponding to the peaks of ROC-LV curves are selected as the appropriate parameters for segmentation. The ESP tool takes advantage of LV to describe the spatial structure of image, and could provide a range of suitable scale parameters for image segmentation. However, the candidate parameter sets are sometimes too large which makes it difficult to select the optimal one. In this case, MMU could be defined as a restriction which determines the smallest size of change area entity to be detected (Desclée et al., 2006; Yue et al., 2012). It is applied to select the most suitable scale parameter based on the results of ESP. Capitalizing on the idea of 'quantile-5' object proposed by Raši et al. (2011), the object sizes are calculated from the smallest scale parameter until at least 95% of the objects are larger than the MMU.

Given the input data, the segmentation for change detection could be carried out in three ways: segmentation using one image only (Raši et al., 2013), segmentation using two images separately, and segmentation using two images stacked together (Niemeyer et al., 2007; Raši et al., 2011). When segmentation using one image only, the segmentation results are assigned to the other image, which lose the spatial information from the second image. Although applying segmentation to two images separately could capture spatial contexts for different dates, it would be difficult to unify two sets of image objects since the shape and size for objects might vary for different time (Niemeyer et al., 2007; Blaschke, 2010). The third segmentation method could consider the characteristics of both images, and generate only one set of segmentation for two images, which could be easily applied for change detection at these two dates. Therefore, we will use this strategy for image segmentation in the proposed framework.

2.2. OB-STVIUM for data blending

The basic idea of OB-STVIUM is to disaggregate the MODIS NDVI time series to the Landsat objects based on the spatial analysis and the linear mixing theory.

Generally, a Landsat image object is an irregular polygon that is not completely covered by a MODIS grid; thus, the spatial analysis is performed to create a bridge layer between the Landsat objects and the MODIS grids (Fig. 2). After segmentation of the Landsat image (Fig. 2(a)), a group of independent objects denoted by O_i are obtained as

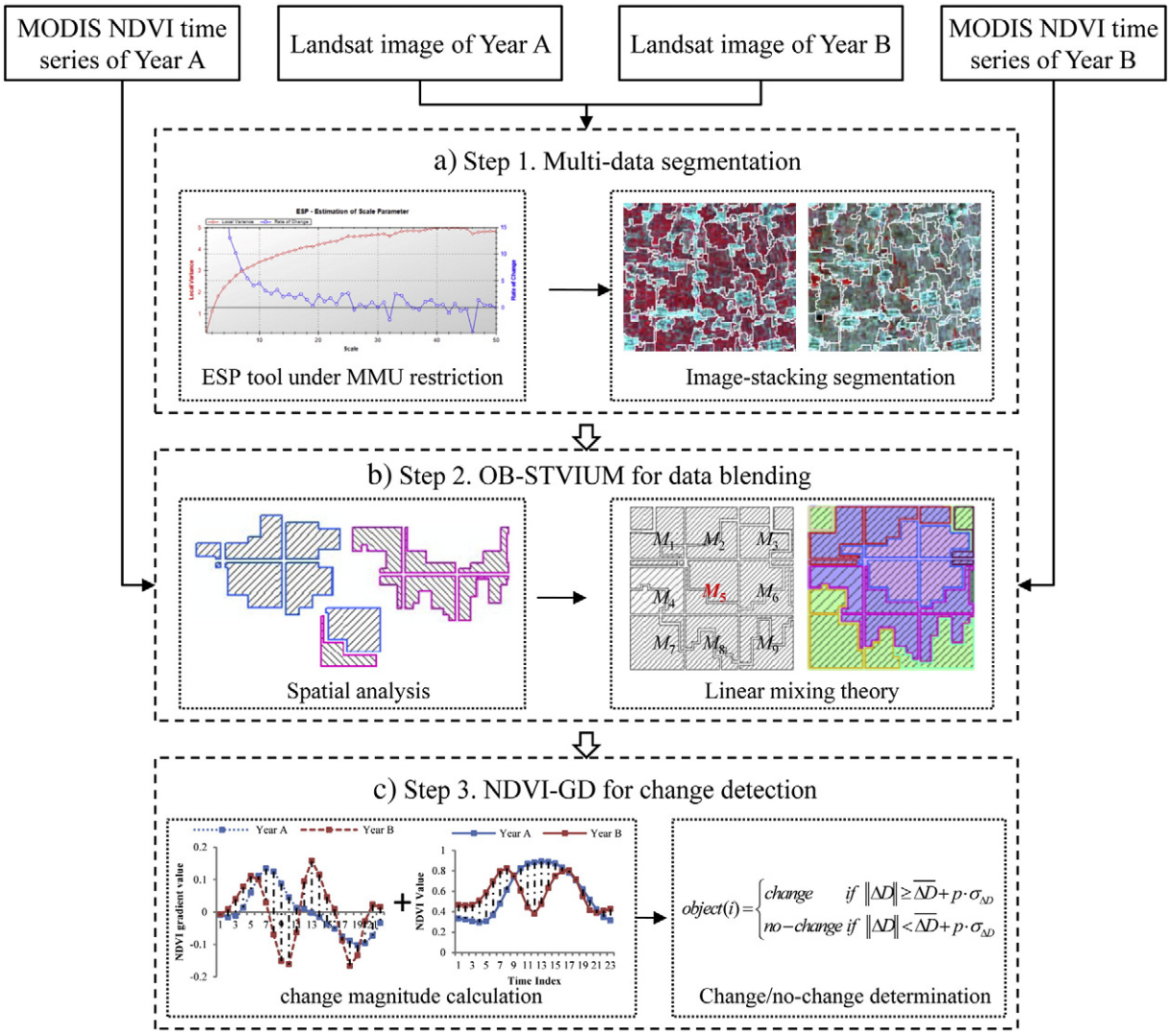

Fig. 1. Framework of the land cover change detection method by integrating OB-STVIUM.

shown in Fig. 2(b). The MODIS image (Fig. 2(c)) is then vectorized into a set of grids described by M_j. (Fig. 2(d)), and NDVI values are assigned to the attribute information of the MODIS grids. Then, a spatial filter is performed to search the MODIS grids that intersect with the target Landsat object. In Fig. 2(e), the light blue and light purple squares identify intersection MODIS grids of object O_4 and O_5 respectively. An intersection calculation between the Landsat object and the corresponding intersection MODIS grids is then performed to obtain the intersection polygon layer. As shown in Fig. 2(f), the blue and purple hatched areas represent the intersection polygons that were derived from object O_4 and O_5 respectively, using the intersection calculation with the corresponding MODIS grids. The intersection polygon is described by (O_i, M_j), where O_i is the object and M_j is the intersecting MODIS grid. Then, the intersection polygons constitute the bridge layer between the Landsat objects and the MODIS grids. As shown in Fig. 2(g), the spatial topology analysis indicates that each Landsat object can be composed of intersection polygons that are completely contained within the Landsat object, as well as MODIS grid. For example, object O_4 consists of the intersecting polygons (O_4, M_1), (O_4, M_2), (O_4, M_3), (O_4, M_4), (O_4, M_5) and (O_4, M_6), and object O_5 is composed of the intersecting polygons (O_5, M_4), (O_5, M_5), (O_5, M_6), (O_5, M_7), (O_5, M_8) and (O_5, M_9). Similarly, the MODIS grid M_5 is composed of (O_4, M_5) and (O_5, M_5).

After the spatial analysis between the Landsat objects and the MODIS grids, it is reasonable to assume that the NDVI value of an object is the linear summation of NDVI values of the intersection polygons within the object weighted by the corresponding percentage coverage (Eq. (1)):

$$NDVI(O_i, t) = \sum_{j=1}^{m} f_o(O_i, M_j) \cdot NDVI(O_i, M_j, t) \quad (1)$$

where $NDVI(O_i, t)$ is the NDVI value of object i at time t; $NDVI(O_i, M_j, t)$ denotes the NDVI value of intersection polygon (O_i, M_j) at time t; and the percentage coverage of the intersection polygon (O_i, M_j) over the object is described by $f_o(O_i, M_j)$. In Eq. (1), the value of $f_o(O_i, M_j)$ can be determined by the ratio of the intersection polygon area to the object area. The value of $NDVI(O_i, t)$ can be determined if $NDVI(O_i, M_j, t)$ is known. Thus, it is necessary to estimate the value of $NDVI(O_i, M_j, t)$. Similarly, the NDVI value of MODIS data at time t, which is denoted by $NDVI(M_j, t)$, can also be aggregated from the NDVI values of the intersection polygons contained in the MODIS grid with the weight of the corresponding percentage coverage:

$$NDVI(M_j, t) = \sum_{i=1}^{n} f_M(O_i, M_j) \cdot NDVI(O_i, M_j, t) \quad (2)$$

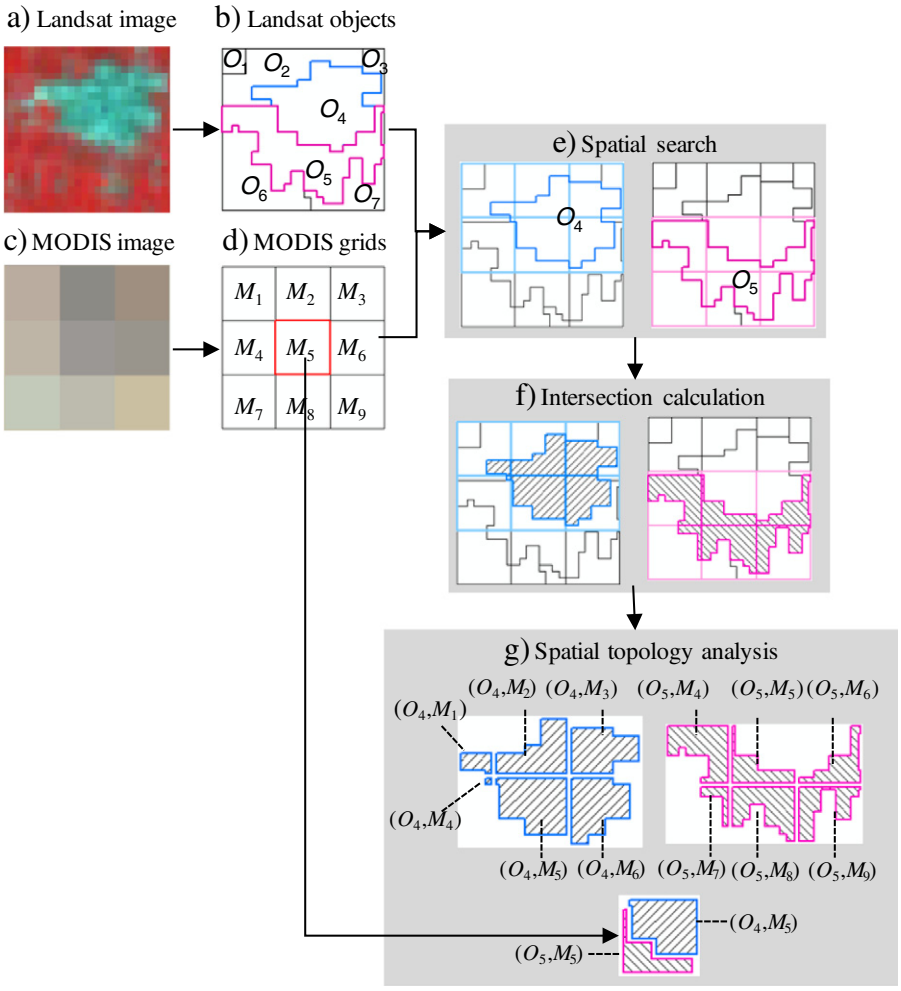

Fig. 2. Flowchart of the spatial analysis between Landsat objects and MODIS grids.

where the value of $f_M(O_i,M_j)$ is the percentage coverage of the intersecting polygon (O_i,M_j) in MODIS grid j, which can be calculated by the ratio of the intersection polygon area to the MODIS grid area. Because the value of $NDVI(M_j,t)$ is known from the MODIS image, it is possible to obtain the value of $NDVI(O_i,M_j,t)$.

In general, the MODIS grid is covered by multiple intersecting polygons, which indicates that a unique solution of $NDVI(O_i,M_j,t)$ cannot be obtained without more information; therefore, the linear mixing theory is used to solve the problem. The principle of this theory is that the NDVI value of a MODIS mixed pixel can be aggregated from the NDVI value of each land cover type weighted by the fractional cover, as shown in Eq. (3):

$$NDVI(M_j,t)=\sum_{k=1}^{h} f(C_k,M_j)\cdot NDVI(C_k,t)+\varepsilon(M_j,t) \tag{3}$$

where $f(C_k,M_j)$ is the area percentage of class C_k in MODIS pixel j; $NDVI(C_k,t)$ is the value of class C_k at time t; $\varepsilon(M_j,t)$ is the corresponding error; and h describes the number of land cover types in MODIS grid i. To solve Eq. (3), a moving window technology is used with the assumption that the neighboring objects of the same class have the similar NDVI values. As shown in Fig. 1(b), the target MODIS grid is M_5, which is the center of the moving window. Based on the object-based unsupervised classification, a linear system of equations is built, as shown in Eq. (4):

$$\begin{pmatrix} NDVI(M_1,t)\\ \vdots\\ NDVI(M_j,t)\end{pmatrix}=\begin{pmatrix} f(C_1,M_1) & \cdots & f(C_k,M_1)\\ \vdots & \ddots & \vdots\\ f(C_1,M_j) & \cdots & f(C_k,M_j)\end{pmatrix}\begin{pmatrix} NDVI(C_1,t)\\ \vdots\\ NDVI(C_k,t)\end{pmatrix}+\begin{pmatrix} \varepsilon(M_1,t)\\ \vdots\\ \varepsilon(M_j,t)\end{pmatrix} \tag{4}$$

Eq. (4) can be solved using the linear least squares method to obtain the value of $NDVI(C_k,t)$. If the intersection polygon (O_i,M_j) belongs to the land cover class C_k, the NDVI value can be estimated as follows:

$$NDVI(O_i,M_j,t)=NDVI(C_k,t) \tag{5}$$

Based on the NDVI value of the intersection polygon, the NDVI values of object i at time t $NDVI(O_i,t)$ can be obtained, as shown in Eq. (1). When the NDVI values at other times are obtained, it is easy to construct the NDVI time series curve of the object.

2.3. NDVI-GD for change detection

Based on the NDVI time series produced by OB-STVIUM, change detection is accomplished by assessing differences of NDVI time series of

the same object at different years. The shape of NDVI time series is important for deriving relevant vegetation phenological characteristics, and NDVI values are indispensable to describe the growth and health of the vegetation (Reed et al., 1994). Therefore, both shape and value differences are important for change detection using NDVI time series. Chen et al. (2013) proposed the Spectral Gradient Difference (SGD) for change detection that described spectral shape differences quantitatively but did not consider differences in reflectance values. Capitalizing on the idea of SGD, the NDVI-GD is proposed in this study to measure the shape and value differences of the NDVI time series by integrating the metric of Euclidean distance.

The NDVI gradient is defined to describe the shape of the NDVI time series quantitatively for each object. First, the NDVI time series is divided into multiple segments for each time step (Fig. 3(a)). In each segment, its NDVI gradient is calculated as shown in Eq. (6), which reflects the trend between the neighboring time indexes:

$$g(i,t_{k-1},t_k)=\frac{NDVI(O_i,t_{k-1})-NDVI(O_i,t_k)}{t_{k-1}-t_k} \tag{6}$$

where $g(i,t_{k-1},t_k)$ is the NDVI gradient from time index t_{k-1} to t_k of object i, and $NDVI(O_i,t_{k-1})$ and $NDVI(O_i,t_k)$ are the NDVI values at time index t_{k-1} and t_k of object i, respectively. Fig. 3(b) shows the NDVI gradients of the original NDVI time series in Fig. 3(a). The value of NDVI gradients should be positive (e.g., $g(i,5,6)$) and increasing when vegetation starts to grow, and it gradually decreases to zero when the vegetation reaches their peak during the growing season. After that, it should decrease to negative (e.g., $g(i,18,19)$) since the vegetation starts to defoliate till the end of the growing season. A greater absolute value of $g(i,t_{k-1},t_k)$ indicates a larger change of NDVI from time index t_{k-1} to t_k. Therefore, the NDVI gradient vector $\mathbf{G}$ (Eq. (7)) combined with the gradients of all time segments could be used to describe the shape of the NDVI time series:

$$\mathbf{G}=(g(i,1,2),g(i,2,3),\ldots,g(i,k-1,k))^T \tag{7}$$

Based on the NDVI gradient calculation, the NDVI gradient difference is used to describe the shape changes of the NDVI time series at different years. It is assumed that the NDVI values of object i at year A and year B are given by $\mathbf{H}$ and $\mathbf{J}$, respectively:

$$\mathbf{H}=(NDVI_h(O_i,t_1),NDVI_h(O_i,t_2),\cdots NDVI_h(O_i,t_k))^T \tag{8}$$

$$\mathbf{J}=(NDVI_j(O_i,t_1),NDVI_j(O_i,t_2),\cdots NDVI_j(O_i,t_k))^T \tag{9}$$

Using Eqs. (8) and (9), the object's NDVI gradient vectors $\mathbf{G_H}$ and $\mathbf{G_J}$ can be obtained. Fig. 1(c) shows the NDVI gradients, and the dashed lines between them indicate the gradient differences. The vector of the NDVI gradient difference $\mathbf{\Delta G}$ measures the differences of the NDVI curve shapes as follows:

$$\begin{aligned}\mathbf{\Delta G}&=\mathbf{G_J}-\mathbf{G_H}\\&=\left(g_j(i,1,2),g_j(i,2,3),\ldots,g_j(i,k-1,k)\right)^T-(g_h(i,1,2),g_h(i,2,3),\ldots,g_h(i,k-1,k))^T\end{aligned} \tag{10}$$

where $g_j(i,k-1,k)$ and $g_h(i,k-1,k)$ are the NDVI gradient values of time segment $(k-1,k)$ at different acquisition time intervals. The absolute value of $\mathbf{\Delta G}$ is calculated to measure the shape differences of the NDVI curves:

$$\|\Delta\mathbf{G}\|=\sum_{m=2}^{k}\left|g_j(i,m-1,m)-g_h(i,m-1,m)\right| \tag{11}$$

The NDVI gradient differences primarily describe the shape differences of the NDVI time series, but they cannot measure the differences of the NDVI value adequately as indicated by the dashed lines between the original NDVI curves in Fig. 1(c). Therefore, the Euclidean distance between two NDVI time series is used to complement the shortage of NDVI gradient differences, as shown in Eq. (12):

$$\|\Delta\mathbf{C}\|=\sqrt{\sum_{n=1}^{k}\left(NDVI_j(O_i,t_n)-NDVI_h(O_i,t_n)\right)^2} \tag{12}$$

where $\|\Delta\mathbf{C}\|$ is the difference of the NDVI value. We combine the shape and value differences of the NDVI time series to assess changes of land cover, as shown in Eq. (13):

$$\Delta D=w_{\|\Delta\mathbf{G}\|}\times\|\Delta\mathbf{G}\|+w_{\|\Delta\mathbf{C}\|}\times\|\Delta\mathbf{C}\| \tag{13}$$

where $w_{\|\Delta\mathbf{G}\|}$ and $w_{\|\Delta\mathbf{C}\|}$ are the weights of $\|\Delta\mathbf{G}\|$ and $\|\Delta\mathbf{C}\|$ respectively, and ΔD is the comprehensive change magnitude. Because the NDVI profile shape and values are equally important, the weights are set both 0.5 in the study. The value of ΔD represents the change possibility of the object, while a larger ΔD value indicates a higher possibility of change.

After calculating the change magnitude, a threshold (T_p) defined by the mean magnitude ($\overline{\Delta D}$) plus an adjustable parameter (p) multiplied by the standard deviation ($\sigma_{\Delta D}$) is used to determine the change and no-change objects (Xian et al., 2009), which is calculated by Eq. (14):

$$T_p=\overline{\Delta D}+p\cdot\sigma_{\Delta D} \tag{14}$$

An optimal searching method is used to automatically determine the parameter p based on training samples. With this, a series of parameters are obtained within a certain range with a fixed step, and the corresponding thresholds are calculated using Eq. (14). Accuracies of change detection results are validated using the training samples, and the

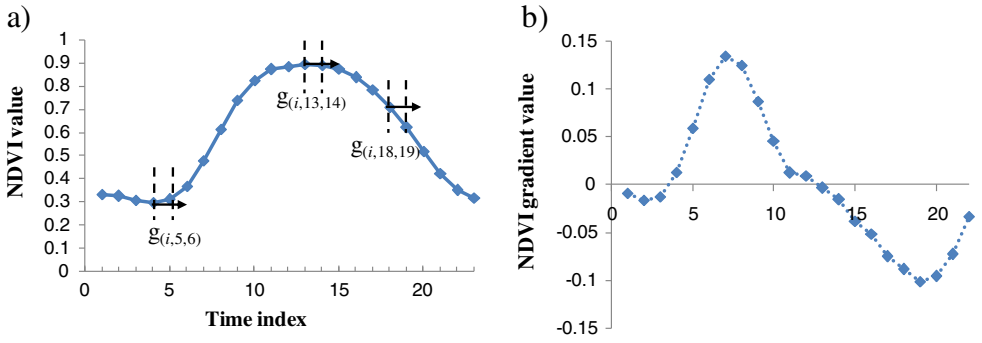

Fig. 3. Calculation of the NDVI gradient: (a) original NDVI curve and (b) NDVI gradients.

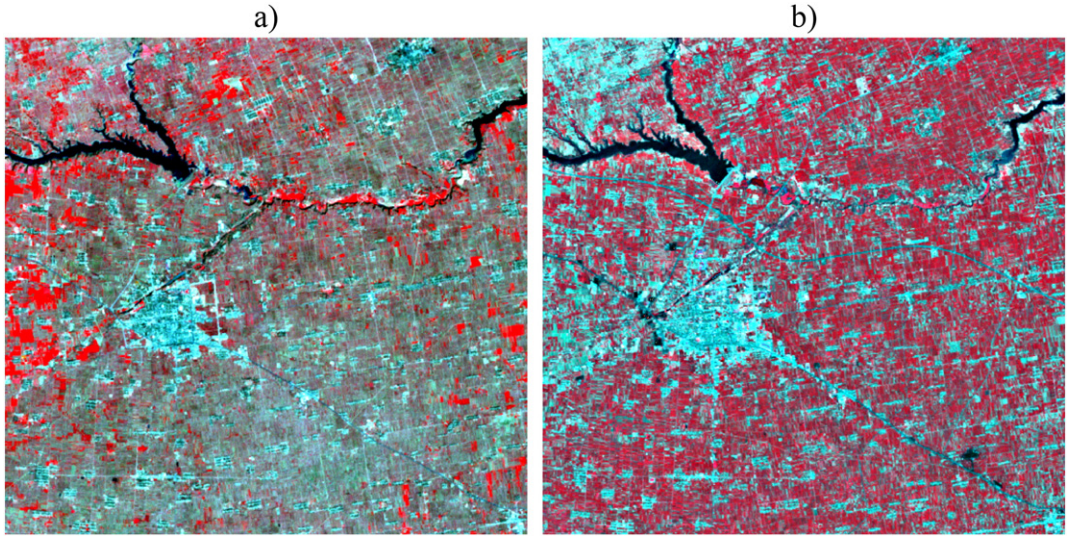

Fig. 4. Landsat images of the study area for change detection (NIR-Red-Green false composition): (a) captured on March 31th, 2002; and (b) captured on June 29th, 2009.

parameter with the highest accuracy is eventually used for change detection.

2.4. Validation strategies

Validation strategies include performance evaluation for data blending and accuracy assessment for change detection.

The performance of data blending is evaluated by comparing the results with the observed MODIS NDVIs and Landsat NDVIs using quality indicators (Gevaert and García-Haro, 2015; Busetto et al., 2008). The performance evaluation by using MODIS NDVIs is based on the concept that the blending NDVIs from disaggregated values according to the linear mixing theory should be equal/close to the original MODIS image (Maselli, 2001; Busetto et al., 2008). The blending NDVIs are resampled to MODIS resolution, and then correlation coefficients (r) (Eq. (15)) and Root Mean Square Errors (RMSE) (Eq. (16)) between blending NDVIs and MODIS NDVIs on the same day are calculated.

$$r = \frac{\sum_{i=1}^{n}\left(NDVI_i^b - \overline{NDVI^b}\right)\left(NDVI_i^o - \overline{NDVI^o}\right)}{\sqrt{\sum_{i=1}^{n}\left(NDVI_i^b - \overline{NDVI^b}\right)^2 \cdot \sum_{i=1}^{n}\left(NDVI_i^o - \overline{NDVI^o}\right)^2}} \quad (15)$$

$$RMSE = \sqrt{\frac{\sum_{i=1}^{n}\left(NDVI_i^b - NDVI_i^o\right)^2}{n}} \quad (16)$$

where $NDVI_i^b$ and $NDVI_i^o$ are the blending and observed NDVI values of pixel i; $\overline{NDVI^b}$ and $\overline{NDVI^o}$ are the mean values of blending and observed NDVI. Although the agreement with MODIS NDVIs can manifest the consistency of algorithm, it cannot imply its reality. Therefore, more Landsat images are collected as a surrogate for field data to test the realistic of blending NDVIs by calculating the correlation coefficient and RMSE between blending NDVIs and Landsat NDVIs on the nearest day.

The accuracy assessment curves and error matrix are used to assess the accuracy of change detection based on the test samples. In general, the results of change detection are dependent on the thresholds of change magnitude. Accuracy assessment curves represent the quantitative relationships between the parameter level for threshold (Eq. (14)) and the accuracy assessment figures (Chen et al., 2013). The curves used here include lines for overall accuracy, Kappa coefficient, change omission and change commission. By doing so, it can better validate the rationality of optimal parameter for threshold calculation. Moreover, the results of change detection with the optimal parameter are assessed by using error matrix based on the test samples.

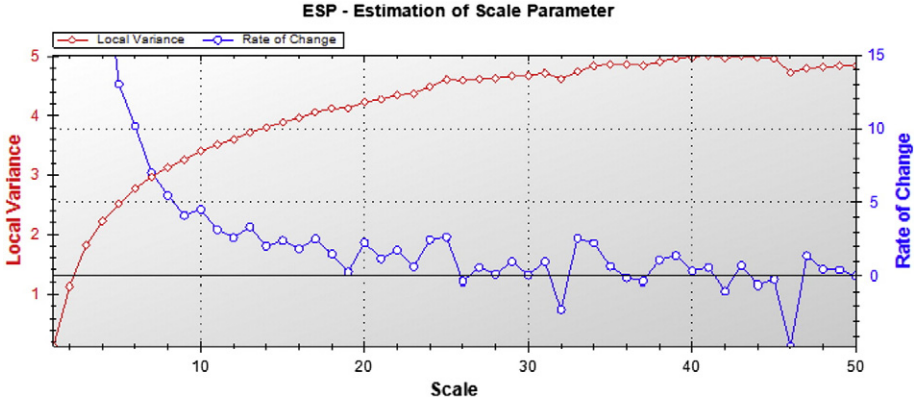

Fig. 5. The LV-ROC graph exported by ESP tool.

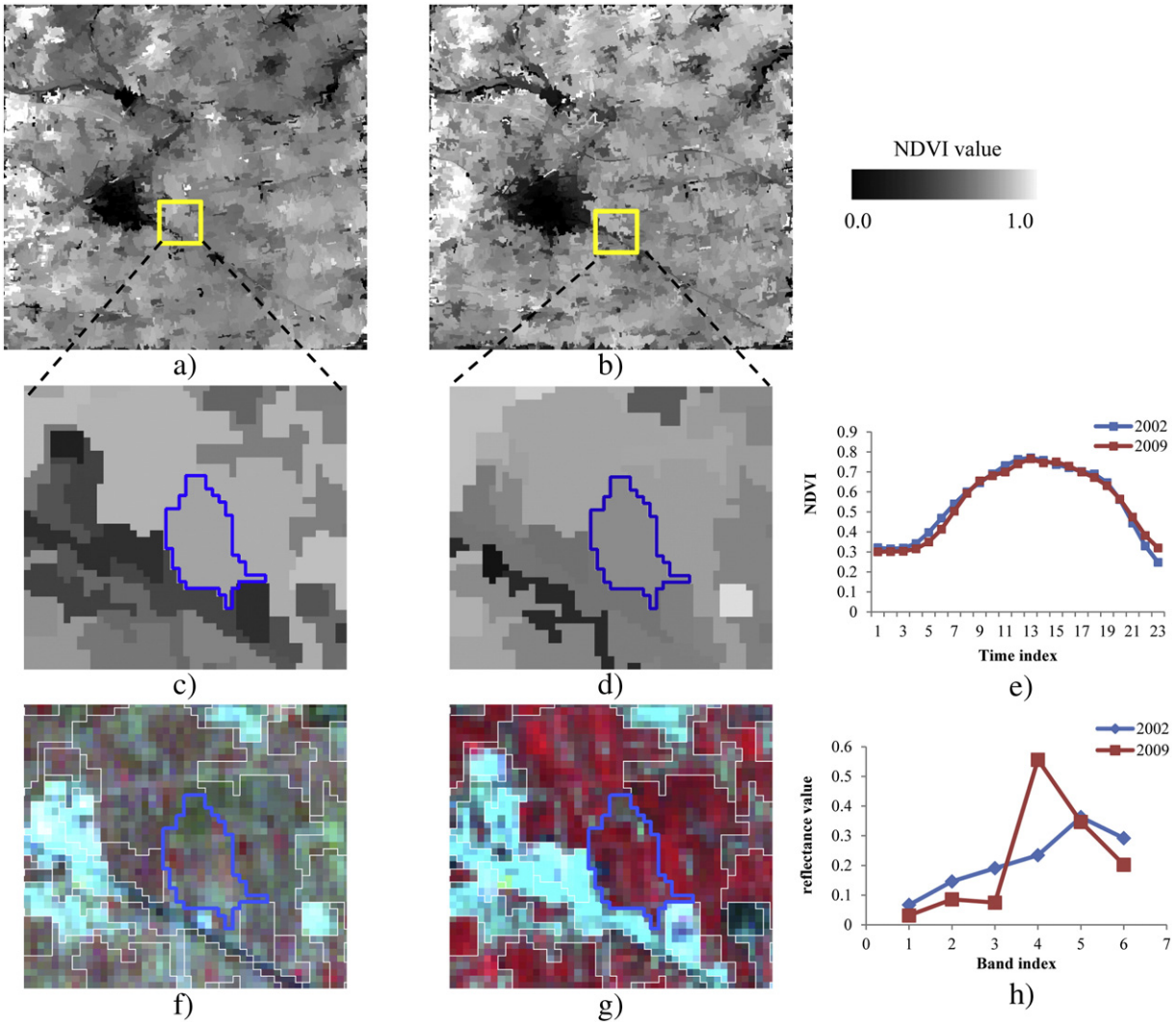

Fig. 6. Comparison of NDVI time series produced by OB-STVIUM and original spectral curves of Landsat images: (a) and (b) are the images of blending NDVI in 2002 and 2009 respectively; (c) and (d) are the amplification regions of the yellow rectangles in (a) and (b); (e) is the NDVI time series of the object described in the blue polygon in (c) and (d); (f) and (g) are the Landsat images of 2002 and 2009 overlaid with objects; (h) shows the spectral curves of the objects described by the blue polygons in (f) and (g).

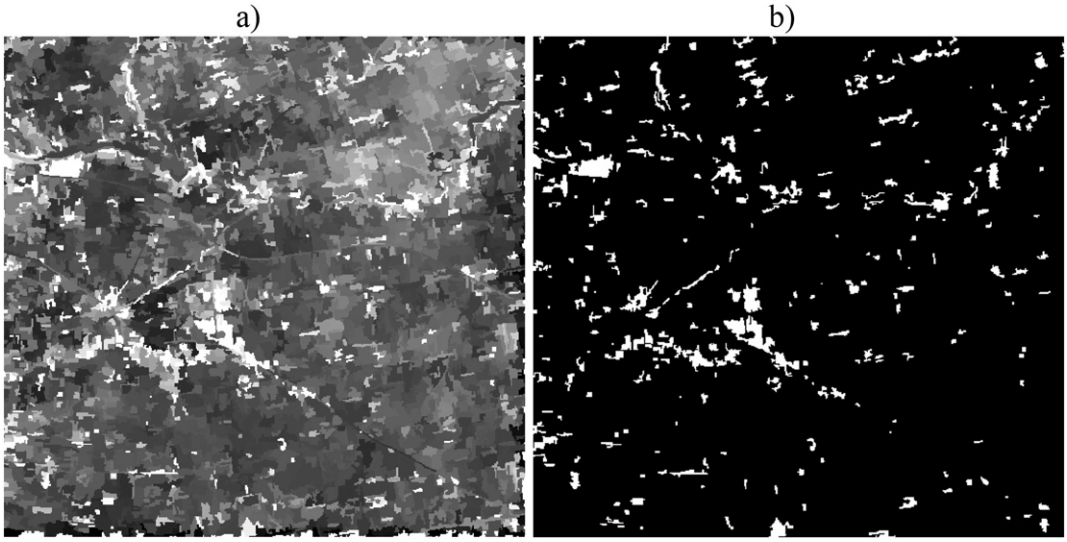

Fig. 7. The change magnitude (a) and change detection results (b) of NDVI-GD.

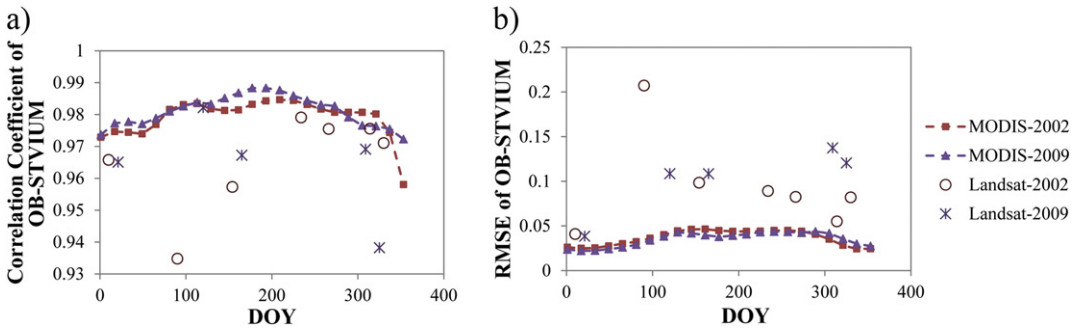

Fig. 8. The evaluation results of OB-STVIUM using correlation coefficient (a) and RMSE (b).

3. Study area and data source

The study area used in this study is located in Liquan County, Shanxi Province, China. It covers approximately 240 km^2 (34°3′35.48″N - 34°5′42.84″N, 108°2′0.44″E - 108°12′33.55″E). The region locates in the warm temperate zone and has four distinct seasons because of the continental monsoon. This area has a variety of land cover types including cropland, building-up, water, bareland and forest. Among these land cover types, the most dominant one is cropland, which could be easily affected by pseudo changes of phenological differences. In addition to the diverse land cover types, predominant land cover change in China has occurred in this region, including extensive urbanization, agricultural field abandonment, and deforestation, which could be used to test the performance of the proposed method across different land cover change types.

A couple of cloud-free Landsat images covering the study area have been obtained from the United States Geological Survey (USGS) website (http://glovis.usgs.gov/) for change detection. The acquisition dates of the images were March 31th, 2002 and June 29th, 2009 from the Landsat-7 and Landsat-5 satellites, respectively. To eliminate the influence of atmospheric conditions, atmospheric corrections were applied to the images using the FLAASH modeling tool in the ENVI software, which incorporates the MODTRAN4 radiation transfer code to convert the digital value in the original image to the surface spectral reflectance. Then, the geometric registration of the two Landsat images was performed with the RMSE of 0.5 pixels to avoid registration errors. Fig. 4 shows the images after data preprocessing and indicates that the spectral features of the vegetation and cropland in the two images are significantly different.

More Landsat images in 2002 and 2009 have also been collected to evaluate the performance of the data blending algorithm. In 2002, six cloud-free Landsat 7 ETM+ images were available including January 10, June 3, August 22, September 23, November 10 and November 26. In 2009, four images were obtained including January 21, June 14, November 5, and November 21. Because there was no cloud free image for spring in 2009, image acquired in April 30, 2010 was added as a substitute. These validation images have also been atmospherically corrected via FLAASH in ENVI software, and then the NDVI images were obtained using red and near infrared bands.

The annual MODIS NDVI 16-day composite grid data (MOD13Q1) of the years 2002 and 2009 were acquired from the Level 1 and Atmosphere Archive and Distribution System (LAADS) Web of National Aeronautics and Space Administration (NASA) (http://ladsweb.nascom.nasa.gov/index.html). The dataset of each year was composed of twenty-three 16-day MODIS NDVI images with a spatial resolution of 250 m in the sinusoidal projection. MODIS NDVI time series images were re-projected from the original sinusoidal projection to the UTM-WGS84 projection to maintain consistency with the Landsat data. The Savitzky-Golay filter was then applied to reduce the noise present in the NDVI time series that was caused primarily by atmospheric variability and cloud contamination (Chen et al., 2004).

The samples were collected for the training of optimal parameter search and the accuracy assessments of change detection. Seed points of samples were first selected using stratified random sampling method, and then the polygon samples with a window size of 3 × 3 pixels were obtained by regional growth with the seed points. With the aid of the high resolution images and reference materials, the polygon samples were labeled as change or no-change. When the number of change or no-change pixels in a polygon sample was more than 6, it was labeled as change or no-change correspondingly, otherwise it was eliminated because it is unable to determine its change status. In total, there were 100 polygon samples (900 pixels) of no-change and 77 polygon samples (693 pixels) of change. 40 Samples of no-change (360 pixels) and 30 samples of change (270 pixels) were used for parameter training, and the rest were used for accuracy validation.

4. Results

4.1. Segmentation of Landsat images

ESP as a customized process was applied in the eCognition software. After setting the algorithm parameters of ESP, the tool calculated the LV of the objects from scale parameter 1 to 50 with step of 1. Based on the ROC curve (Fig. 5), 10, 13, 20, 25, 33, 39 and 47 were selected as the potential scales which corresponds to local maxima (i.e., notable local peaks in Fig. 5). The MMU was defined as 1 ha according to the change fragmentation in the study area. Because the alternative scales obtained by ESP tool were larger or equal 10 and the smaller scale parameters were insufficient, two smaller scale parameters 5 and 7 were added as alternative according to the MMU. Then, we calculated the object sizes and the percentages of size larger than MMU from scale 5. It was found that the scale parameter 10 reached the MMU size criterion for the 'quantile-5' object, which was then selected as the optimal scale parameter for segmentation.

The Landsat images acquired in March 31th, 2002 and June 29th, 2009 were stacked, and then the multi-resolution segmentation with scale parameter 10 was performed in eCognition software. The segmentation parameters of the shape and compactness were 0.1 and 0.1 respectively through experience. After the segmentation, the object

Table 1
Error matrix of the change detection.

		Reference change			
		Change	No-change	Sum	Commission error
Classified change	Change	353	36	389	9.25%
	No-change	70	504	574	12.20%
	Sum	423	540	963	
	Omission error	16.55%	6.67%		

Overall accuracy = 88.99%, Kappa coefficient = 0.77.

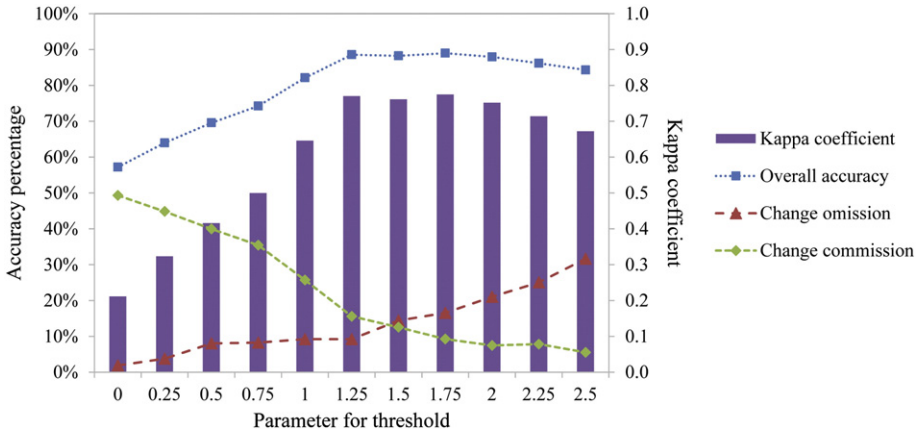

Fig. 9. Accuracy assessment curves with parameters ranging from 0 to 2.5.

layers with the attributes of mean spectral value in each object of the two Landsat images were exported.

4.2. NDVI time series construction

OB-STVIUM was used to construct the NDVI time series of the Landsat objects in 2002 and 2009. In order to get the object classification results, the object-based ISODATA unsupervised classification was conducted with a predefined class number of 5, because the primary land cover types in the study area are cropland, building-up, water, bareland and forest. The results of OB-STVIUM in 2002 and 2009 are shown in Fig. 6(a) and (b). Because the original Landsat images were acquired in different seasons, the same object of different years expressed different spectral features as shown in Fig. 6(h). Therefore, if the Landsat images were used for change detection, the pseudo changes caused by phenological differences could be inevitable. On the contrary, the NDVI time series for the year of 2002 and 2009 appear to be very similar (Fig. 6(e)); therefore, it is reasonable to consider that OB-STVIUM could potentially eliminate the pseudo changes caused by phenological differences.

4.3. Identification of change and no-change areas

The NDVI-GD change detection method was used to calculate the change magnitude of the NDVI time series in each object. As shown in Fig. 7(a), the brighter area of the change magnitude indicates a higher change possibility. The parameter searching based on the training samples was used to determine the optimal parameter for change detection. Existing studies demonstrated that the optimal range of adjustable parameter is from 0 to 2.5 (Morisette and Khorram, 2000; Xian et al., 2009). Following this, a series of parameters under this range were obtained with the step of 0.01. Then the overall accuracy based on the training samples of change detection with the corresponding threshold was calculated. The parameter 1.67 achieved the highest overall accuracy, which was then used for the final change detection. As shown in Fig. 7(b), the change detection result is expressed as a binary image where the white and black areas indicate the change and no-change areas respectively.

4.4. Validation results

The performance evaluation of data blending algorithm was accomplished by comparing with original MODIS NDVIs and Landsat NDVIs (Fig. 8). Because NDVI is mainly used to indicate the vegetation greenness and vigor, the land cover types of water and building-up were excluded. Correlation coefficients between NDVIs of OB-STVIUM and original MODIS range from 0.958 to 0.988 and RMSEs vary from 0.022 to 0.046. The correlation coefficients with Landsat NDVIs are lower than MODIS NDVIs, which range from 0.934 to 0.982. The RMSEs compared with Landsat NDVIs are from 0.038 to 0.137, which are higher than the ones compared with MODIS. Therefore, the NDVIs of OB-STVIUM are more similar with MODIS NDVIs compared with Landsat NDVIs. This is because the theoretical basis of OB-STVIUM, which using linear mixing theory disaggregates the MODIS NDVI to the Landsat object, causes it to produce MODIS-like NDVIs.

The error matrix based on test samples was employed to assess the accuracy of change detection results using the parameter 1.67. As shown in Table 1, the overall accuracy is 88.99%, and the Kappa coefficient is 0.77, which demonstrates the good performance of the object-based change detection results.

Because the change detection accuracy assessment is dependent on the threshold of change magnitude, the accuracy assessment curve

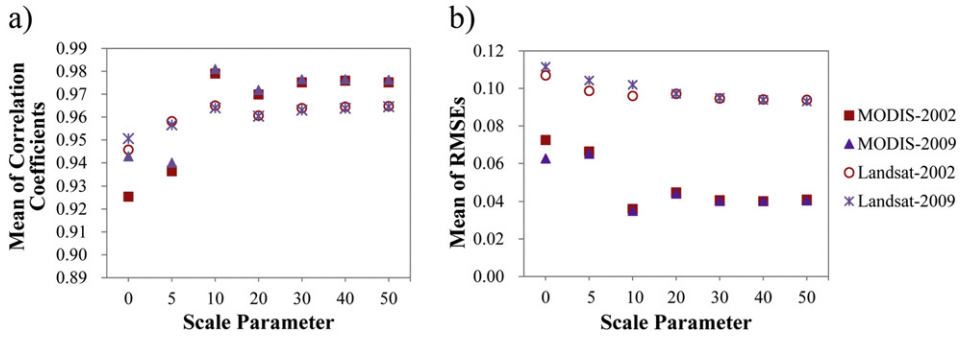

Fig. 10. Mean of correlation coefficients (a) and RMSEs (b) with various segmentation scales.

Table 2
The parameter for threshold and accuracy assessment features.

Segmentation scale	Parameter for threshold	Overall accuracy	Kappa coefficient	Change omission	Change commission
0	1.09	73.21%	0.44	46.81%	21.05%
5	1.03	77.78%	0.54	30.97%	22.13%
10	1.67	88.99%	0.77	16.55%	9.25%
20	1.25	75.70%	0.50	35.93%	23.23%
30	1.16	68.22%	0.33	55.32%	27.59%
40	0.49	61.79%	0.20	57.45%	40.98%
50	1.29	63.55%	0.21	68.32%	31.63%

based on the test samples was used to assess the influences of thresholds on change detection. The parameters of threshold, ranging from 0 to 2.5 with 0.25 step, were first set to obtain a series of change detection results. The accuracy assessment curves including Kappa coefficient, overall accuracy, change omission and change commission are shown in Fig. 9. The parameters between 1.5 and 1.75 obtain the highest Kappa coefficient and overall accuracy, and have the best trade-off between change omission and commission. The optimal parameter 1.67 based on the training samples was in this range, which means the parameter optimization is effective.

5. Discussion

5.1. Effects of the input parameters on the algorithm performance

In this section, we analyzed the effects of two input parameters including segmentation scale and window size on the algorithm performance.

Since the scale parameter determines the size of objects, it will affect the results of data blending and final change detection. In order to examine its impact on the performance of OB-STVIUM, segmentation scales 0, 5, 10, 20, 30, 40, and 50 were used to derive different results, while results of segmentation scale 0 are equivalent to the pixel-based results. The correlation coefficients and RMSEs between blending NDVIs and MODIS NDVIs at the same day were calculated, and then the mean values of correlation coefficients and RMSEs were obtained to evaluate the consistency accuracy of data blending at each segmentation scale (Fig. 10(a)). Similarly, the mean correlation coefficients and RMSEs between blending NDVIs and Landsat NDVIs were calculated to assess the reality accuracy of blending results (Fig. 10(b)). From Fig. 10, the mean correlation coefficients increase significantly, and the means RMSEs decrease sharply when the scale increase from 0 to 10. After that, both RMSEs and correlation coefficients fluctuate slightly when segmentation scale increases from 10 to 50. Therefore, it is reasonable to conclude that the object based data blending is superior to the pixel based one, and OB-STVIUM is less sensitive to larger segmentation scale to some extent. Meanwhile, the segmentation scale of 10 appears to be the optimal scale for the data blending because of its higher correlation coefficients and lower RMSEs, which manifests that ESP under MMU restrictions is an effective method to determine the optimal scale for data blending.

Based on results of OB-STVIUM with various segmentation scales, the change magnitude results by using NDVI-GD were also obtained at various segmentation scale, and the optimal parameter search based on the same training samples was performed to determine the thresholds for change detection, as shown in Table 2. All change detection results were assessed using the same test samples, and the overall accuracy, Kappa coefficient, change omission and change commission are described in Table 2. From scale 0 to 10, the values of the overall accuracy and Kappa coefficient increase, which is consistent with the assessments of OB-STVIUM (Fig. 10). However, the accuracy indicators decrease gradually when scale parameter continues to increase after 10. One potential reason is that there might be mixed large objects containing both change and no-change areas when the segmentation scale is too large, thus making it difficult to distinguish change and no-change areas. This is more serious when segmentation scale exceeds the real object scale in the landscape (e.g., size of croplands). Compared with the results of object-based data blending model, object-based change detection is more sensitive to segmentation scales.

In addition, we also test the impacts of the moving window size on OB-STVIUM, which is used to solve the linear mixing model (Eq. (4)). OB-STVIUM was conducted using four window sizes including 3×3, 5×5, 7×7 and 9×9 with segmentation scale 10. Fig. 11 shows the mean correlation coefficients and RMSEs of various window sizes compared with original MODIS NDVIs in 2009. The results suggest that the performance of OB-STVIUM degrades when the window size increases. When the window size is too large, more MODIS pixels are involved for the solution of linear system. However, the assumption that the neighboring objects of the same class have the similar NDVI values may be invalid and cause larger errors in the blending results. In this study, the window size of 3×3 is optimal for OB-STVIUM, as suggested for example in Rao et al. (2015).

5.2. Comparisons of data blending algorithms

The performance of OB-STVIUM has also been compared with STARFM and NDVI-LMGM, two different pixel based data blending methods. STARFM and NDVI-LMGM have been applied to produce the 30 m NDVI time series data in 2002 and 2009 using the same input data as OB-STVIUM. The correlation coefficients and RMSEs of STARFM to the original datasets are shown in Fig. 12(a) and (b) respectively. Fig. 12(c) and (d) show the correlation coefficients and RMSEs between NDVI-LMGM and original datasets. The mean correlation coefficients and RMSEs in 2002 and 2009 are shown in Table 3. Based on these comparisons, the mean correlation coefficients of OB-STVIUM are higher than other two methods, while the mean RMSEs are lowest. Therefore, OB-STVIUM has a superior performance compared with other two methods.

OB-STVIUM is an unmixing-based algorithm that disaggregates MODIS NDVI time series to Landsat objects using the spatial analysis

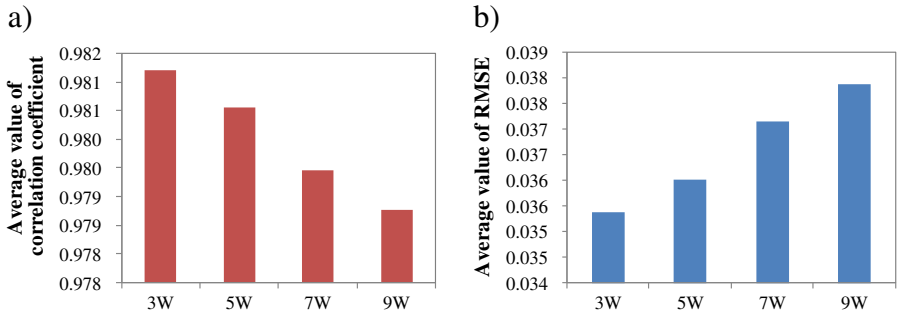

Fig. 11. Mean values of correlation coefficient (a) and RMSE (b) of various window sizes.

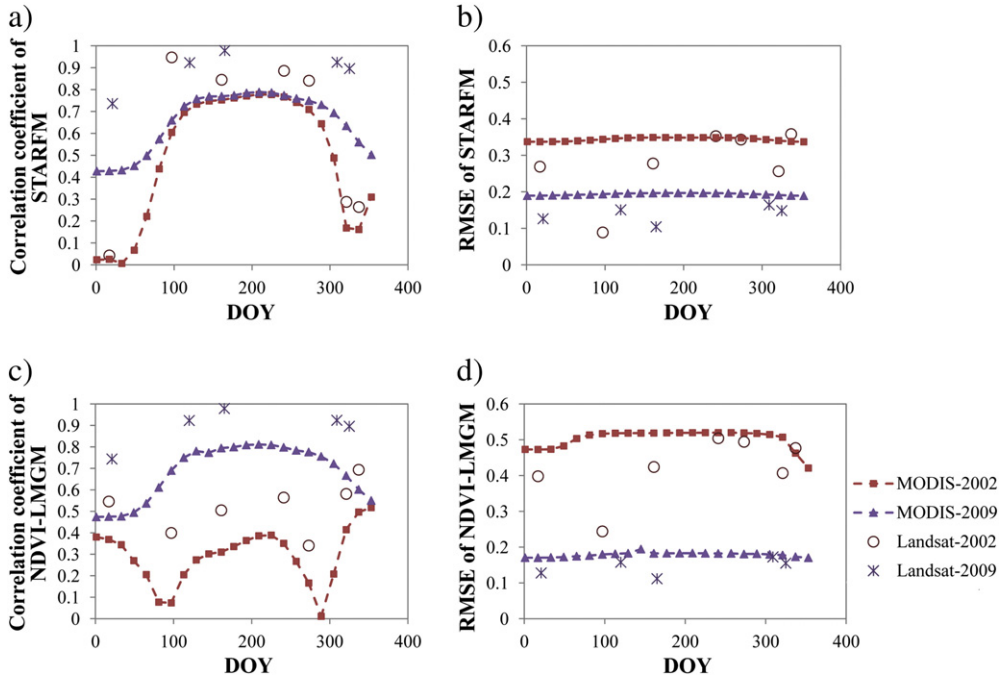

Fig. 12. The evaluation results of STARFM and NDVI-LMGM: (a) correlation coefficients of STARFM, (b) RMSEs of STARFM, (c) correlation coefficients of NDVI-LMGM, (d) RMSEs of NDVI-LMGM.

and the linear mixing theory. The results of OB-STVIUM are MODIS-like NDVI; therefore, the correlations of OB-STVIUM to MODIS imageries of 2002 and 2009 are higher than the Landsat imageries (Table 3). OB-STVIUM utilizes the Landsat image to provide information including spatial pattern and fraction cover of land cover class, and it is less depended on the number and acquisition time of Landsat image; therefore, the differences of mean correlation coefficients and RMSEs to Landsat imageries between 2002 and 2009 are slightly smaller compared with STARFM and NDVI-LMGM.

Different from OB-STVIUM, the basic theories of STARFM and NDVI-LMGM make them to product Landsat-like NDVIs, which are more dependent on the number and acquired time of Landsat images (Gao et al., 2006; Rao et al., 2015; Gevaert and García-Haro, 2015). Their results have higher correlation coefficients and lower RMSEs for the Landsat images than the MODIS images (Table 3 and Fig. 12). Previous studies have pointed out that STARFM and NDVI-LMGM are more dependent on the number of input Landsat-MODIS data pairs, since more available input data pairs could provide more reliable base information to improve the performances of STARFM and NDVI-LMGM (Rao et al., 2015; Gevaert and García-Haro, 2015). However, in this paper, due to only one Landsat image for the construction of NDVI temporal profiles, the performances of STARFM and NDVI-LMGM methods are poorer than OB-STVIUM. Meanwhile, STARFM and NDVI-LMGM are sensitive to the acquisition time of input Landsat images. The Landsat image of 2009 (June 29th) is acquired in the middle of the growing season with stable NDVI; therefore, it could provide more accurate base information on the land cover type and reduce the propagation of predicted error. On the contrary, the Landsat image in March 31th 2002 was acquired at the beginning of the growing season when vegetation is hard to be distinguished from other land covers, which provides inaccurate based information for the prediction. Therefore, the correlation coefficients of STARFM and NDVI-LMGM in 2009 are higher than 2002, while the RMSEs of 2009 are lower than 2002 (Fig. 12 and Table 3).

In general, the selection of optimal data blending method depends on the intended application (Gevaert and García-Haro, 2015). The aim of this paper is to eliminate the pseudo changes caused by the pair images acquired from different seasons. OB-STVIUM method is more appropriate for this application because it is less sensitive to the number and acquired time of Landsat images and can produce MODIS-like NDVIs. On the contrary, STARFM and NDVI-LMGM are more dependent on the input Landsat data. The performances of these two methods are poorer than OB-STVIUM when using only one Landsat image. Meanwhile, the NDVI temporal profiles in different years derived from the two methods may be varied if the pair images are acquired from different seasons, and introduce more errors for change detection.

6. Conclusion

In this study, a new object-based data blending method OB-STVIUM has been developed for land cover change detection to eliminate pseudo changes caused by phenological differences. ESP tool under MMU restriction is employed to obtain the optimal scale for image stacking segmentation for both Landsat images. Then, the OB-STVIUM disaggregates MODIS NDVIs to the Landsat object using spatial analysis and linear mixing theory. Lastly, the NDVI-GD change detection is used to identify the change and no-change objects based on the shape and value

Table 3
The average values of quality indicators in 2002 and 2009.

	2002				2009			
	$\bar{r}_{Lansat}$	$\overline{RMSE}_{Landsat}$	$\bar{r}_{MODIS}$	$\overline{RMSE}_{MODIS}$	$\bar{r}_{Lansat}$	$\overline{RMSE}_{Landsat}$	$\bar{r}_{MODIS}$	$\overline{RMSE}_{MODIS}$
OB-STVIUM	0.965	0.096	0.979	0.036	0.964	0.102	0.981	0.035
STARFM	0.587	0.278	0.495	0.343	0.891	0.138	0.653	0.193
NDVI-LMGM	0.518	0.421	0.291	0.503	0.893	0.144	0.684	0.178

differences of the NDVI time series. The approach was tested in the study area in Liquan County, Shanxi Province, China. The results indicated that the proposed approach can effectively solve the pseudo changes and improve the accuracy of change detection.

An object is the basic unit of the image analysis in this paper. The segmentation scale was determined by ESP tool under MMU restriction which combines the advantages of ESP tool and MMU criterion. With the optimal segmentation scale 10, the blending results have higher correlation coefficients and lower RMSEs to the original MODIS NDVIs and Landsat NDVIs. Meanwhile, the accuracy of change detection results with scale 10 were higher than other scales. Therefore, ESP tool under MMU restriction is an effective method to automatically provide optimal scale for object-based image analysis. When the segmentation scale is 0, namely pixel-based analysis, the accuracies of data blending and change detection are lower; thus it is reasonable to consider that object-based method can improve the accuracy for change detection.

OB-STVIUM employs spatial analysis and linear mixing theory to disaggregate the MODIS NDVI time series to Landsat objects, and produces MODIS-like NDVIs which have higher consistency with original MODIS time series. Compared with STARFM and NDVI-LMGM, it is less dependent on the number and acquisition time of Landsat image, and has superior and stable performances when only one Landsat image was available. Therefore, OB-STVIUM is more suitable for change detection application to eliminate pseudo changes caused by phenological differences.

NDVI-GD change detection is used to determine the change and no-change areas based on the NDVI shape and value differences simultaneously. The NDVI gradient is defined to describe the shape differences of the NDVI time series quantitatively, and Euclidean distance is used to measure the NDVI value differences. The two change metrics complement each other and can obtain a better change detection result. NDVI-GD is more sensitive to the segmentation scale compared with OB-STVIUM, because if the segmentation scale is too large, the change and no-change areas may be contained within one object, and it is difficult to distinguish them.

Although OB-STIVIUM was tested based on Landsat and MODIS data, both could also be easily extended to other data sources, such as SPOT/VEGETATION and Chinese HJ-1B. Therefore, additional experiments are required to improve the proposed method using various sensors in the future. Meanwhile, NDVI-GD was primarily used for identifying change and no-change areas without considering the types of change that occurred. In the future, the proposed method should be developed to determine change types using the change patterns between land cover types based on the NDVI time series of object.

Acknowledgements

This study was partially funded by the National Natural Science Foundation of China (No. 41501483) and Research Foundation for Mapping Geographic Information Public Welfare of China (No. 201512028).

References

Ban, Y., Jacob, A., 2013. Object-based blending of multitemporal multi-angle ENVISAT ASAR and HJ-1 multispectral data for urban land-cover mapping. IEEE Trans. Geosci. Remote Sens. 51 (4), 1998–2006.
Ban, Y., Gong, P., Giri, C., 2015. Global land cover mapping using Earth observation satellite data: recent progresses and challenges. ISPRS J. Photogramm. Remote Sens. 103, 1–6.
Benz, U.C., Hofmann, P., Willhauck, G., Lingenfelder, I., Heynen, M., 2004. Multi-resolution, object-oriented fuzzy analysis of remote sensing data for GIS-ready information. ISPRS J. Photogramm. Remote Sens. 58, 239–258.
Blaschke, T., 2010. Object based image analysis for remote sensing. ISPRS J. Photogramm. Remote Sens. 65, 2–16.
Bodart, C., Eva, H., Beuchle, R., Raši, R., Simonetti, D., Stibig, H.J., et al., 2011. Pre-processing of a sample of multi-scene and multi-date Landsat imagery used to monitor forest cover changes over the tropics. ISPRS J. Photogramm. Remote Sens. 66, 555–563.
Bontemps, S., Bogaert, P., Titeux, N., Defourny, P., 2008. An object-based change detection method accounting for temporal dependences in time series with medium to coarse spatial resolution. Remote Sens. Environ. 112, 3181–3191.
Bontemps, S., Herold, M., Kooistra, L., van Groenestijn, A., Hartley, A., Arino, O., et al., 2012a. Revisiting land cover observation to address the needs of the climate modeling community. Biogeosciences 9, 2145–2157.
Bontemps, S., Langner, A., Defourny, P., 2012b. Monitoring forest changes in Borneo on a yearly basis by an object-based change detection algorithm using SPOT-VEGETATION time series. Int. J. Remote Sens. 33 (15), 4673–4699.
Boschetti, L., Roy, D.P., Justice, C.O., Humber, M.L., 2015. MODIS-Landsat blending for large area 30 m burned area mapping. Remote Sens. Environ. 161, 27–42.
Busetto, L., Meroni, M., Colombo, R., 2008. Combining medium and coarse spatial resolution satellite data to improve the estimation of sub-pixel NDVI time series. Remote Sens. Environ. 112, 118–131.
Chen, J., Jönsson, P., Tamura, M., Gua, Z., Matsushitab, B., Eklundhd, L., 2004. A simple method for reconstructing a high-quality NDVI time-series data set based on the Savitzky–Golay filter. Remote Sens. Environ. 91, 332–344.
Chen, G., Hay, G.J., Carvalho, L.M.T., Wulder, M.A., 2012. Object-based change detection. Int. J. Remote Sens. 33 (14), 4434–4457.
Chen, J., Lu, M., Chen, X., Chen, J., Chen, L., 2013. A spectral gradient difference based approach for land cover change detection. ISPRS J. Photogramm. Remote Sens. 85, 1–12.
Chen, G., Zhao, K., Powers, R., 2014. Assessment of the image misregistration effects on object-based change detection. ISPRS J. Photogramm. Remote Sens. 87 (1), 19–27.
Chen, J., Chen, J., Liao, A., Cao, X., Chen, L., Chen, X., et al., 2015a. Global land cover mapping at 30 m resolution: A POK-based operational approach. ISPRS J. Photogramm. Remote Sens. 103, 7–27.
Chen, X., Yang, D., Chen, J., Cao, X., 2015b. An improved automated land cover updating approach by integrating with downscaled NDVI time series data. Remote Sens. Lett. 6 (1), 29–38.
Coppin, P., Jonckheere, I., Nackaerts, K., Muys, B., Lambin, E., 2004. Review Article Digital change detection methods in ecosystem monitoring: a review. Int. J. Remote Sens. 25 (9), 1565–1596.
Desclée, B., Bogaert, P., Defourny, P., 2006. Forest change detection by statistical object-based method. Remote Sens. Environ. 102, 1–11.
Drăguţ, L., Tiede, D., Levick, S.R., 2010. ESP: a tool to estimate scale parameter for multiresolution image segmentation of remotely sensed data. Int. J. Geogr. Inf. Sci. 24 (6), 859–871.
Gao, F., Masek, J., Schwaller, M., Hall, F., 2006. On the blending of the Landsat and MODIS surface reflectance: predicting daily Landsat surface reflectance. IEEE Trans. Geosci. Remote Sens. 44 (8), 2207–2218.
Gevaert, C.M., García-Haro, F.J., 2015. A comparison of STARFM and an unmixing-based algorithm for Landsat and MODIS data blending. Remote Sens. Environ. 156, 34–44.
Gong, J., Sui, H., Sun, K., Ma, G., Liu, J., 2008. Object-level change detection based on full-scale image segmentation and its application to Wenchuan earthquake. Sci. China, Ser. E: Technol. Sci. 51 (2), 110–122.
Hansen, M.C., Loveland, T.R., 2012. A review of large area monitoring of land cover change using Landsat data. Remote Sens. Environ. 122, 66–74.
Hilker, T., Wulder, M.A., Coops, N.C., Linke, J., McDermid, G., Masek, J.G., et al., 2009. A new data blending model for high spatial- and temporal-resolution mapping of forest disturbance based on Landsat and MODIS. Remote Sens. Environ. 113, 1613–1627.
Hu, Q., Wu, W., Xia, T., Yu, Q., Yang, P., Li, Z., et al., 2013. Exploring the use of google earth imagery and object-based methods in land use/cover mapping. Remote Sens. 5, 6026–6042.
Hussain, M., Chen, D., Cheng, A., Wei, H., Stanley, D., 2013. Change detection from remotely sensed images: from pixel-based to object-based approaches. ISPRS J. Photogramm. Remote Sens. 80, 91–106.
Im, J., Jensen, J.R., Tullis, J.A., 2008. Object-based change detection using correlation image analysis and image segmentation. Int. J. Remote Sens. 29 (2), 399–423.
Jia, K., Liang, S., Zhang, N., Wei, X., Gu, X., Zhao, X., et al., 2014. Land cover classification of finer resolution remote sensing data integrating temporal features from time series coarser resolution data. ISPRS J. Photogramm. Remote Sens. 93, 49–55.
Jin, S., Yang, L., Danielson, P., Homer, C., Fry, J., Xian, G., 2013. A comprehensive change detection method for updating the National Land Cover Database to circa 2011. Remote Sens. Environ. 132, 159–175.
Kovalskyy, V., Roy, D.P., 2013. The global availability of Landsat 5 TM and Landsat 7 ETM + land surface observations and implications for global 30 m Landsat data product generation. Remote Sens. Environ. 130, 280–293.
Lhermitte, S., Verbesselt, J., Jonckheere, I., Nackaerts, K., Aardt, J., Verstraeten, W.W., et al., 2008. Hierarchical image segmentation based on similarity of NDVI time series. Remote Sens. Environ. 112, 506–521.
Lu, M., Wu, W., Zhang, L., Liao, A., Peng, S., Tang, H., 2016. A comparative analysis of five global cropland datasets in China. Sci. China Earth Sci. 59, 1–12.
Maselli, F., 2001. Definition of spatially variable spectral endmembers by locally calibrated multivariate regression analyses. Remote Sens. Environ. 75, 29–38.
Mora, B., Tsendbazar, N.E., Herold, M., Arino, O., 2014. Global land cover mapping: Current status and future trends. In: Manakos, I., Braun, M. (Eds.), Land Use and Land Cover Mapping in Europe: Practices and Trends. Springer, Netherlands, pp. 11–30.
Morisette, J.T., Khorram, S., 2000. Accuracy assessment curves for satellite-based change detection. Photogramm. Eng. Remote. Sens. 66, 875–880.
Niemeyer, I., Marpu, P.R., Nussbaum, S., 2007. Change detection using the object features. IEEE International Geoscience and Remote Sensing Symposium. IEEE, pp. 2374–2377.
Pohl, C., Van Genderen, J.L., 1998. Multisensor image blending in remote sensing: concepts, methods and applications. Int. J. Remote Sens. 19 (5), 823–854.
Powers, R.P., Hay, G.J., Chen, G., 2012. How wetland type and area differ through scale: a GEOBIA case study in Alberta's Boreal Plains. Remote Sens. Environ. 117, 135–145.

Rao, Y., Zhu, X., Chen, J., Wang, J., 2015. An improved method for producing high spatial-resolution NDVI time series datasets with multi-temporal MODIS NDVI data and Landsat TM/ETM+ images. Remote Sens. 7, 7865–7891.
Raši, R., Bodart, C., Stibig, H.J., Eva, H., Beuchle, R., Carboni, S., et al., 2011. An automated approach for segmenting and classifying a large sample of multi-date Landsat imagery for pan-tropical forest monitoring. Remote Sens. Environ. 115, 3659–3669.
Raši, R., Beuchle, R., Bodart, C., Vollmar, M., Seliger, R., Achard, F., 2013. Automatic updating of an object-based tropical forest cover classification and change assessment. IEEE J. Sel. Top. Appl. Earth Obs. Remote Sens. 6 (1), 66–73.
Reed, B.C., Brown, J.F., Vanderzee, D., Loveland, T.R., Merchant, J.W., Ohlen, D.O., 1994. Measuring phenological variability from satellite imagery. J. Veg. Sci. 5 (5), 703–714.
Sun, J., Wu, W., Tang, H., Liu, J., 2015. Spatiotemporal patterns of non-genetically modified crops in the era of expansion of genetically modified food. Sci. Rep. 5.
Tewkesbury, A.P., Comber, A.J., Tate, N.J., Lamb, A., Fisher, P.F., 2015. A critical synthesis of remotely sensed optical image change detection techniques. Remote Sens. Environ. 160, 1–14.
Wu, W., Verburg, P.H., Tang, H., 2014. Climate change and the food production system: impacts and adaptation in China. Reg. Environ. Chang. 14, 1–5.
Xian, G., Homer, C., Fry, J., 2009. Updating the 2001 National Land Cover Database land cover classification to 2006 by using Landsat imagery change detection methods. Remote Sens. Environ. 113, 1133–1147.
Yang, J., Gong, P., Fu, R., Zhang, M., Chen, J., Liang, S., et al., 2013. The role of satellite remote sensing in climate change studies. Nat. Clim. Chang. 3 (10), 875–883.
Yu, Q., Wu, W., Verburg, P.H., Vliet, J.V., Yang, P., Zhou, Q., et al., 2013. A survey-based exploration of land-system dynamics in an agricultural region of northeast China. Agric. Syst. 121, 106–116.
Yue, A., Yang, J., Zhang, C., Su, W., Yun, W., Zhu, D., et al., 2012. The optimal segmentation scale identification using multispectral Worldview-2 images. Sens. Lett. 10, 285–291.
Zhang, J., 2010. Multi-source remote sensing data fusion: status and trends. International Journal of Image & Data Fusion 1 (1), 5–24.
Zhu, X., Chen, J., Gao, F., Chen, X., Masek, J.G., 2010. An enhanced spatial and temporal adaptive reflectance blending model for complex heterogeneous regions. Remote Sens. Environ. 114 (11), 2610–2623.